JMEPEG (2009) 18:548–553
DOI: 10.1007/s11665-009-9425-7

1059-9495/$19.00

Properties of Co-alloyed Ni-Fe-Ga Ferromagnetic Shape Memory Alloys

V.A. Chernenko, K. Oikawa, M. Chmielus, S. Besseghini, E. Villa, F. Albertini, L. Righi, A. Paoluzi, P. Müllner, R. Kainuma, and K. Ishida

(Submitted October 17, 2008; in revised form January 29, 2009)

It is experimentally found that in the $Ni_{54}Fe_{20-x}Co_xGa_{26}$ ferromagnetic shape memory alloys, Co variation from 0 to 9 at.% leads to: (i) almost linear change of martensitic transformation temperatures from −70 °C to 120 °C; (ii) a non-monotonous change of the Curie temperature, and (iii) a linear decrease of saturation magnetization from 60 to 43 Am^2/kg. The selected alloys grown as single crystals have been (magneto-) mechanically tested. The superelastic effect has been measured to be about 4%. The magneto-strain shows a training effect which is an evidence of the effect of magnetic-field-induced twin-boundary motion.

Keywords intermetallics, material selection, mechanical testing

1. Introduction

In the ferromagnetic thermoelastic martensites, such as those exhibited by prototype off-stoichiometric Ni_2MnGa alloys, the ordinary magnetostriction can trigger the twin boundary motion whereby giant magnetic-field-induced strains are obtained (see, e.g., Ref 1 and references therein). The same level of strains can also be obtained in these alloys using thermal and/or mechanical activation, as in the usual non-ferromagnetic shape memory materials. Such multi-functionality, important for applications, motivates a worldwide activity related to the development of ferromagnetic shape memory alloys (FSMAs), particularly based on the off-stoichiometric Heusler alloys (Ref 1-3). The Ni-Fe-Ga alloys (Ref 4-6), like the other Mn-free Heusler FSMAs, are found to be much more ductile than the classical Ni-Mn-Ga. The improved mechanical properties of these alloys are mainly due to the presence of the γ-phase precipitates. The disadvantage of ternary Ni-Fe-Ga FSMAs is related to the impossibility to use them at room temperature owing to the reduced Curie temperature of the austenite. Preliminary studies show that Co affects significantly the transformation temperatures and magnetic properties of Ni-Fe-Ga alloys: both, the martensitic transformation temperature, T_M, and Curie temperature, T_C, increase and the saturation magnetization, I_s, decreases with increasing Co-content in the series of $Ni_{51}Fe_{22-x}Co_xGa_{27}$ alloys. On the other hand, an increase of Co concentration in the series of $Ni_{54-x}Fe_{19}Co_xGa_{27}$ alloys causes increase in T_C and I_s and decrease in T_M (Ref 7, 8). In both cases, Co-content varies between 0 and 6 at.%.

In this article, the investigation is extended to the probing Ni-Fe-Ga FSMAs with different base compositions and doped by Co up to 9 at.%. The influence of Co on the transformation behavior is determined and selected compositions are studied in a single crystalline form to demonstrate the functional capacity of these alloys.

2. Experimental

$Ni_{54}Fe_{20-x}Co_xGa_{26}$ alloys, with x = 0, 2, 3, 4, 6, 8, and 9 at.%, labeled as Co0…Co9, were prepared as 20-g buttons by arc-melting of high purity elements and subsequent five-times re-melting. The samples cut of each alloy were sealed in a quartz ampoule with argon atmosphere and solution treated at 1100 °C for 24 h followed by a water-quench. Then, the samples were sealed in the quartz capsule again and aged at 650 °C for 100 h followed by a water-quench. More details about the sample preparation can be found in Ref 6. Scanning electron microscopy observations of aged samples confirmed that the β-phase matrix contains γ-phase precipitates as observed in similar alloys in some studies (Ref 4-8). Using x-ray powder diffraction, it was found that the alloys in a bulk are highly textured. In order to perform structural analysis, the grinding procedure of powder preparation and the abovementioned heat treatment was applied. The forward (on cooling), T_M, and reverse (on heating), T_A, martensitic transformation (MT) temperatures were determined as the peak positions on the calorimetric curves measured with a rate of 5 °C/min by a

This article is an invited paper selected from presentations at Shape Memory and Superelastic Technologies 2008, held September 21-25, 2008, in Stresa, Italy, and has been expanded from the original presentation.

V.A. Chernenko, S. Besseghini, and **E. Villa**, IENI, CNR, Corso Promessi Sposi, 29, Lecco 23900, Italy; **K. Oikawa, R. Kainuma,** and **K. Ishida**, Department of Materials Science, Graduate School of Engineering, Tohoku University, Aoba-yama 6-6-02, Sendai 980-8579, Japan; **M. Chmielus**, Department of Materials Science and Engineering, Boise State University, Boise, ID 83725 and Helmholtz Centre Berlin for Materials and Energy, Glienicker str.100, 14109 Berlin, Germany; **P. Müllner**, Department of Materials Science and Engineering, Boise State University, Boise, ID 83725; **F. Albertini** and **A. Paoluzi**, IMEM, CNR, Parco Area delle Scienze 37/A, Parma 43010, Italy; **L. Righi**, Dipartimento di Chimica GIAF, Parco Area delle Scienze 17/A, Parma 43100, Italy. Contact e-mail: vladimir.chernenko@gmail.com.

Table 1 Compositions, heat treatment, crystal orientation and martensitic (T_M, T_A), and Curie (T_C) transformation temperatures of single crystals used for mechanical and magneto-mechanical tests

Single crystal	Composition, at.%				Heat treatment	Lattice orientation along tensile axis	Transformation temperatures, °C		
	Ni	Fe	Ga	Co			T_M	T_A	T_C
#1	52.4	23.2	24.4	···	As-grown	···	−45	−20	51
#2	53.0	12.0	26.9	8.1	1100 °C for 24 h +650 °C 100 h	···	20	65	42
#3	50.0	17.0	27.0	6.0	As-grown	⟨10 6 13⟩	45	55	70

standard DSC analyzer. The Curie temperature, T_C, and saturation magnetization, I_s, ($T = -196$ °C, $H = 1$T) were measured by an in-house made low-field magnetic susceptibility set-up and a vibrating sample magnetometer (VSM), respectively.

Two single crystalline alloys #1 and #2 of 80 g each were grown by Bridgman method in an alumina crucible using previously produced induction-melted ingots. The single crystalline wires of alloy #3 were grown by pulling-down of the melt from the orifice of the alumina crucible with a rate about 1 mm/min in the micro-PD furnace (Ref 9). The wires were 1.5 mm in diameter and up to 200 mm in length. The compositions of alloys #1 and #2 were determined with uncertainty of 0.2% by X-ray fluorescent analysis, while EDX was used for the analysis of alloy #3 made with uncertainty of 0.5%. Table 1 shows the compositions, heat treatments, orientations, and transformation temperatures of the single crystalline samples. The values of the transformation temperatures for alloys #2 and #3 indicate that they can be considered as possible room-temperature FSMAs.

A DMA Q800 analyzer was utilized to register from the same sample the temperature dependencies of elastic modulus E (T) and internal friction (IF), tan δ, in the dynamic tensile mode, as well as stress versus strain, σ-ε, at a constant temperature in the static tensile mode. The dynamic measurements were carried out at a frequency of 1 Hz, an oscillation strain amplitude of 10^{-4}, and temperature rate of 2 °C/min. In the static mechanical tests, the upper limit of load and the stress change rate were 18 N and 2.5 MPa/min, respectively.

The alloy #2 and wire #3 were tested at room temperature in the Dynamical Magneto-Mechanical Testing Device (DMMT). Prior to these tests, the samples were heated above MT temperature, loaded by constant stress of 20-50 MPa and cooled to the martensitic state. The samples were glued on one end to the sample holder specially designed to prevent a possible wire bending. The magneto-mechanical measurements are made with a constant magnetic field of 0.97 T which was rotated with 29 revolutions per minute during the strain measurements, and with up to 5,000 revolutions per minute during the period between the measurements. The test was continued up to one million magneto-mechanical cycles. Experimental details are given in (Ref 10, 11).

3. Structural Behavior and Transformation Characteristics

Previous structural studies have shown that the martensitic structure formed in Ni-Fe-Ga(Co) alloys depends on the degree of B2/$L2_1$ atomic order (Ref 6) and/or the amount of Co (Ref 9). In particular, it was found that the lower degree of the atomic order and/or higher content of Co favor the formation of non-modulated 2M-martensite. It is also worth noting that a mixture of martensitic phases with modulated or non-modulated structure is frequently observed in FSMA Heusler alloys (Ref 12).

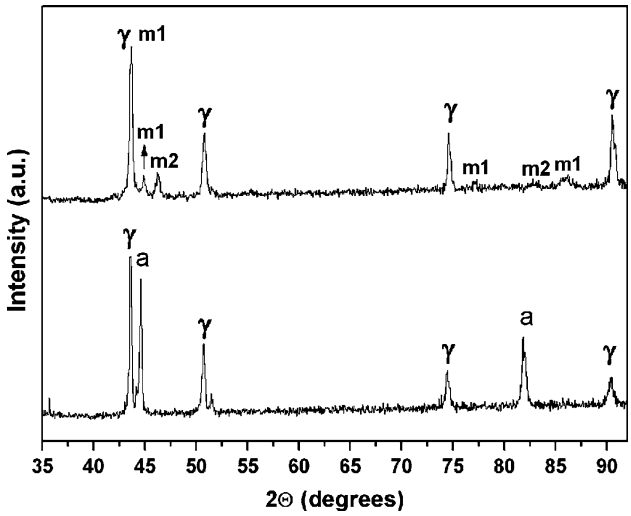

Fig. 1 XRD patterns of powdered and heat-treated sample of Co2 alloy at 20 °C (lower curve) and at −193 °C (upper curve) collected using CuK_α radiation. The peaks are attributed to two martensites, m1 and m2; austenite, a; and γ-phase

In this study, x-ray analysis was hindered by a strong texture of the alloys in bulk form. Moreover, the powder samples appeared to be enriched by γ-phase depressing peaks of the other phases as it is evident from Fig. 1. As an example, Fig. 1 shows x-ray diffraction patterns of the Co2 sample obtained at 20 °C (lower curve) and at −193 °C (upper curve). Obviously, the results such as shown in Fig. 1 do not allow a reliable structural analysis of the phases. Nevertheless, they contain some useful informations which can be deduced by taking into account the literature data (e.g., Ref 13). Particularly, the Co2 sample presents about 30 vol.% of austenitic phase at 20 °C with a lattice parameter of 0.5756 nm. The γ-phase has a unit cell parameter of 0.3601 nm. By lowering the temperature (to −193 °C), the austenitic reflections are replaced by few new peaks related to the two martensitic phases (m1 and m2 in Fig. 1). Presumably, crystal lattices of these martensites could be attributed to the basic monoclinic and tetragonal unit cells exhibiting different types of the lattice modulations (e.g., Ref 12, 13). With an increasing Co-content, alloys show a

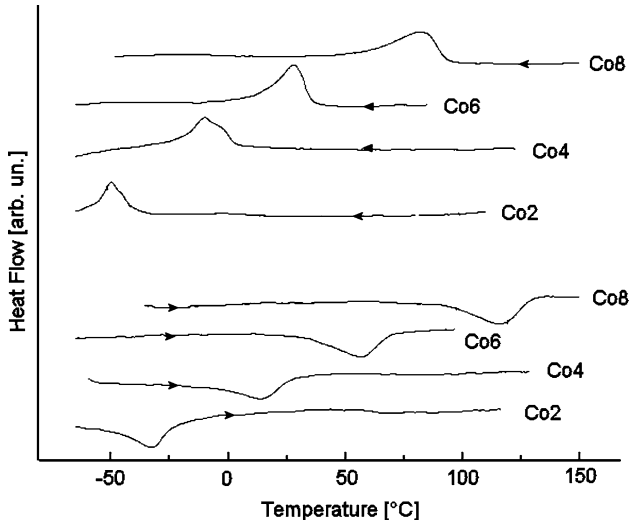

Fig. 2 Typical heating-cooling DSC curves for $Ni_{54}Fe_{20-x}Co_xGa_{26}$ alloys

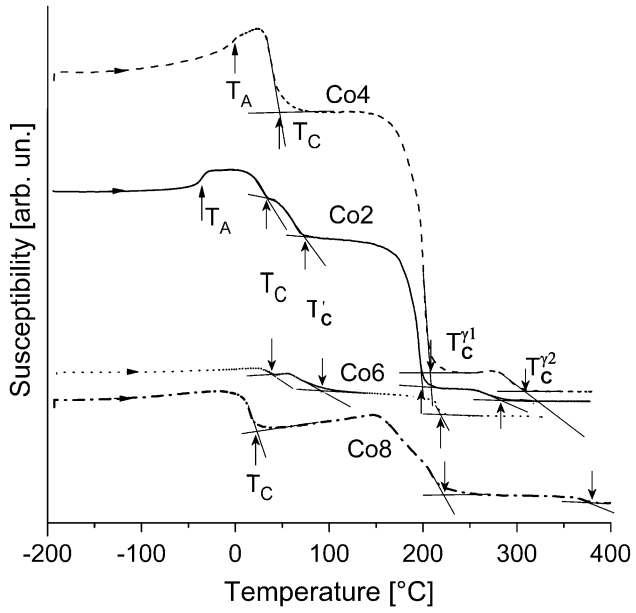

Fig. 3 Typical heating curves of low-field magnetic susceptibility for $Ni_{54}Fe_{20-x}Co_xGa_{26}$ alloys. The reverse MT temperature, T_A, and Curie temperatures T_C, T'_C, $T_C^{\gamma 1}$, and $T_C^{\gamma 2}$ are indicated by vertical arrows. The reverse MT temperature can only be detected when $T_A < T_C$. T_C is attributed to B2/$L2_1$-ordered matrix, $T_C^{\gamma 1}$ and $T_C^{\gamma 2}$ observed above 200 °C in all the alloys are tentatively attributed to the two γ-phases (γ1 and γ2), respectively. T'_C observed in Co2 and Co6 alloys can be related either to the magnetic inhomogeneities of matrix or different martensitic phases. One cannot exclude also a possible presence of the third γ-phase

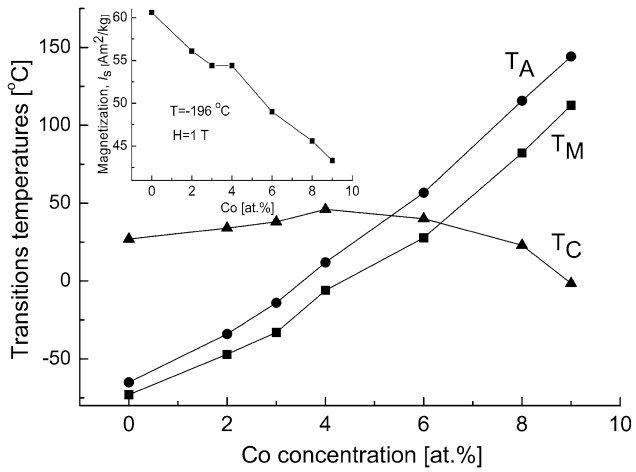

Fig. 4 Characteristic temperatures of martensitic transformation and Curie temperature as a function of Co-content for the $Ni_{54}Fe_{20-x}Co_xGa_{26}$ alloys. *Inset*: Co-concentration dependence of saturation magnetization value measured at −196 °C in 1 T magnetic field. Curves are guides for the eye

larger amount of γ-phase. Alongside the predominant γ1-phase with a = 0.360 nm, an additional γ2-phase with a = 0.3544 nm appears.

Typical DSC heating and cooling curves and typical heating curves of low-field magnetic susceptibility, χ(T), for $Ni_{54}Fe_{20-x}Co_xGa_{26}$ alloys are shown in Fig. 2 and 3. Curves in these figures allow the determination of characteristic transformation temperatures, such as T_M and T_A corresponding to the maximum values on the cooling and heating DSC curves, respectively (Fig. 2) and tangentially defined Curie temperatures T_C corresponding to the B2/$L2_1$-ordered matrix phase and, at least, two to the γ-phases (Fig. 3). The DSC curves yield the average transformation heat of MT equal to 1.8 ± 0.6 J/g for all the alloy series. This average value is provided because the experimental composition dependence of the transformation heat is irregular.

The χ(T) curves show distinctive anomalies produced by the reverse MT only when condition $T_A < T_C$ holds, alloys Co2…Co4 in Fig. 3. The curves in Fig. 3 reflect a non-homogeneous character of the alloys exhibiting at least two additional anomalies above 200 °C for all the alloys studied which can naturally be attributed to the Curie temperatures of the two γ-phases found by x-ray diffraction. In the Co2 and Co6 alloys, an additional anomaly at T'_C appears which could be thought as produced by some magnetic inhomogeneities of matrix or a possible presence of the third γ-phase with its Curie temperature. Note that the multiple anomalies at χ(T) curves were observed for ternary Ni-Fe-Ga alloys (Ref 14), which were attributed to the Curie temperatures of γ-phases.

The characteristic temperatures, T_M and T_A, and Curie temperature, T_C, determined from Fig. 2 and 3 are plotted in Fig. 4 as a function of Co-content. As in the case of other Co-doped Ni-Fe-Ga alloys (Ref 7), T_M and T_A show a strong increase when Co substitutes Fe whereas, contrary to Ref 7, T_C exhibits a diffuse maximum at about 4 at.%. Note that a similar behavior of T_C is also observed for Ni-Mn-Ga alloys and their Co-doped analogs, which was explained by the influence of electron concentration and Mn occupation of different sites in the lattice (Ref 15). Furthermore, T_A and T_M dependencies in Fig. 4 demonstrate a considerable and monotonous increase of the temperature hysteresis of MT as a function of Co-doping. This evolution can be attributed to the increasing volume fraction of γ-phase precipitates and decreasing mobility of the interfaces. Incidentally, this increase does not seem to affect the Co-concentration dependence of total magnetic moment as the experimental results in the Inset to Fig. 4 evidence. Here,

the linear dependence could mean that the contribution of γ-phase to total magnetic moment is relatively the same in all alloys studied.

The studies of Co-doping on the transformation characteristics have shown that in this particular Ni-Fe-Ga alloy one can design an alloy with room-temperature ferromagnetic martensite at a narrow Co-content window located in the vicinity of 4.5 at.% (Fig. 4).

4. Elastic and Superelastic Properties

Dynamic and quasi-static mechanical properties have been studied in tensile mode for the single crystalline samples shown in Table 1. The cooling/heating temperature dependencies of elastic modulus and tan δ are shown in Fig. 5 for two samples. The results for sample #3 are not shown due to the similar behavior as #1. In samples #1 and #3, the elastic modulus exhibits a low value in all the temperature ranges with a deep minimum at T_M (on the cooling curve) and at T_A (on the heating curve) corresponding to the highest rate of the temperature change of tan δ produced by MT. Besides, quite strong modulus softening of about 1.3 MPa/K is observed for alloys #1 and #3 in the cubic phase. In contrast, alloy #2 shows a high value of elastic modulus accompanying by a low level of internal friction. All the other features mentioned for samples #1 and #3 are not so pronounced in the alloy #2. Both, the almost three times larger modulus and multiple difference in tan δ between the samples and #2 and #3, suggest a strong stiffening of the matrix in alloy #2, presumably, due to heat treatment accompanied by a disperse hardening.

Quasi-static stress-strain, σ-ε, measurements at different constant temperatures have been performed previously for alloy #3 (Ref 9). In this study, Fig. 6 depicts the typical tensile stress-strain dependencies for alloy #1 obtained in the martensitic and austenitic states in the stress range up to 160 MPa which is our instrumental limitation. Incidentally, in this stress range, alloy #2 did not show a superelasticity effect. In the austenitic state, the σ-ε dependencies for alloy #1, indeed, exhibit a reversible superelastic strain of about 4.0% produced by a stress-induced martensitic transformation with a stress hysteresis of 50 MPa (Fig. 6). The superelastic strain value, although being influenced by the presence of non-transformed γ-phase (Ref 16, 17), is comparable with the crystallographically estimated value when tensile axis is along ⟨100⟩ (Ref 16). The plateau-like accumulation of the superelastic strain is steep in Fig. 6 because in the alloys containing precipitates, a considerable hardening occurs during MT (see also Ref 16, 17). The yield stress in the martensitic state is quite high due to a reduced mobility of interfaces which are possibly pinned by precipitates.

Figure 7 shows the temperature dependence of critical stress determined by a tangential method from the stress-strain curves (Ref 17). The data points in Fig. 7 can be approximated by the two straight lines with the slopes of 1.0 and 0.5 MPa/K. As far as the data points in Fig. 7 are reproducible, one can attribute the first line to the low-stress-induced martensitic phase being identical to thermally induced one, while the second line is assumed to belong to the high-stress-induced martensitic phase with different crystallographic structure. Previous structural studies revealed that the thermally induced martensitic phase in alloys similar to alloy #1 can be described as a monoclinic 7M-structure (Ref 18, 19). The crystallographic identification

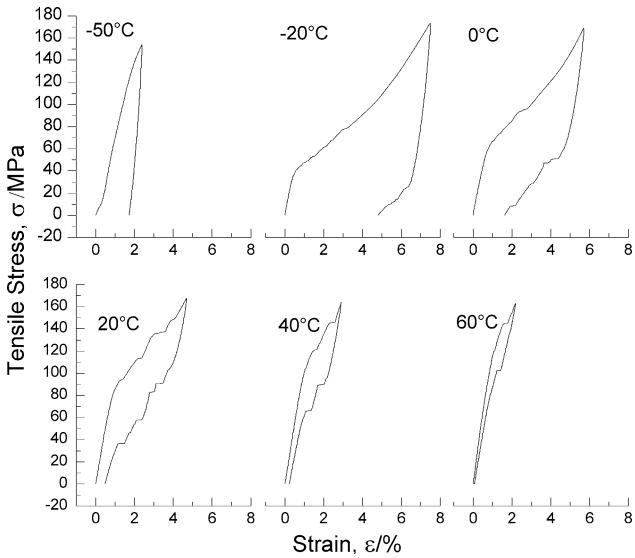

Fig. 6 Tensile stress-strain dependencies for alloy #1

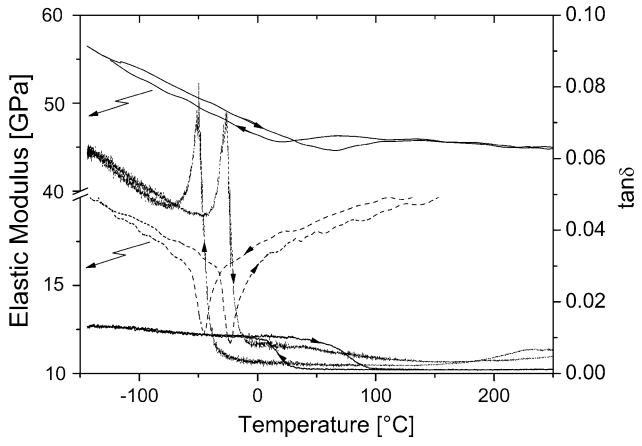

Fig. 5 Heating-cooling temperature dependencies of elastic modulus and internal friction of alloy #1 (dashed line) and alloy #2 (full line)

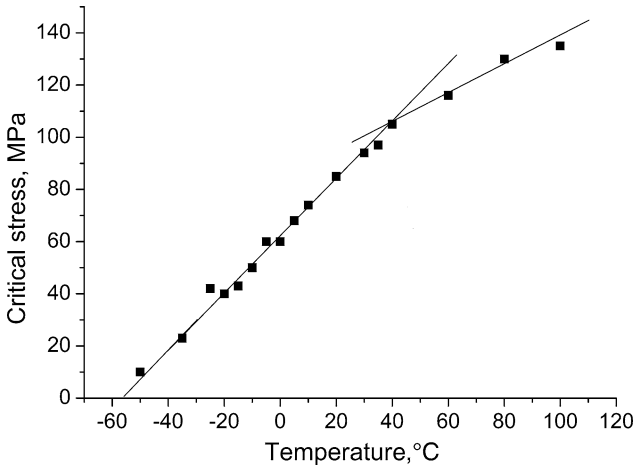

Fig. 7 Tensile critical stress vs. temperature phase diagram of alloy #1. Linear approximations of the data points are used

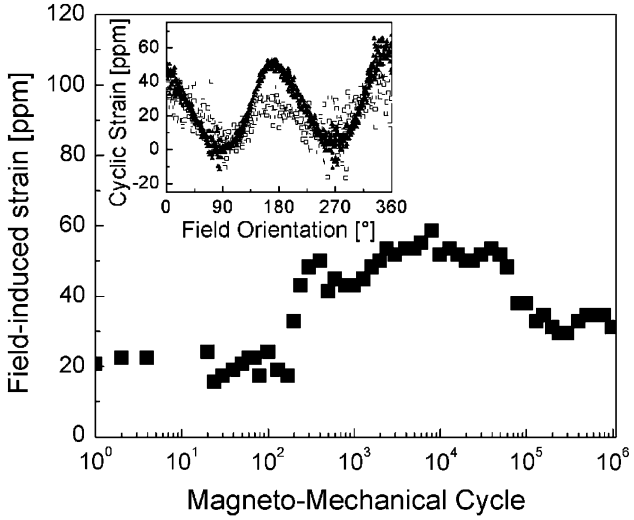

Fig. 8 Field-induced strain as a function of the number of magneto-mechanical cycles. The magnetic field-induced strain as a function of field direction at cycle 6 (open squares) and at cycle 16,000 (full triangles) are shown in the inset

of second stress-induced martensitic phase needs separate studies. With regard to the results for the single crystalline Ni-Fe-Ga alloy (Ref 18), the formation of a tetragonal $L1_0$ martensite is anticipated in this case.

Since the critical stress versus temperature dependence was shown experimentally to be a function of volume fraction of γ-phase (Ref 17), in this study, we refrain from the thermodynamic estimations using Clausius-Clapeyron relationship. The results of the mechanical testing confirm an assessment that the FSMAs can also be competitive in their functional properties typical for the ordinary shape memory alloys.

5. Magnetostrain Properties

Magnetostrain response was studied for the ferromagnetic martensitic phases of alloys #2 and #3 which were suitable for room-temperature-operating DMMT.

The magnetic field-induced strain (MFIS) of sample #3 was measured over 1 million magneto-mechanical cycles. The measured signal was with a maximum of 34 increments close to the detection limit. However, a cyclic strain change of a sample was detected and is shown in Fig. 8 for cycle 6 and 16,000. It can be seen that the shape of the detected MFIS periodic signal is not changing. The strain percent scattering recorded during the first 200 cycles was approximately ±10 ppm of the total cyclic strain and with increasing cycles numbers, it decreased to less than ±5 ppm. The highest strain corresponds to a magnetic field direction parallel to the axis of the wire #3, e.g., at 0° and 180°. As seen in Fig. 8, the MFIS during the initial 200 cycles was around 20 ppm and than tripled over the next 10,000 cycles to 60 ppm. After 40,000 cycles, a decrease of strain to about 40 ppm occurs and then remains constant at about 30 ppm over the next 950,000 cycles until the experiment was stopped at one million cycles.

In the magnetostrain measurements up to 6,000 field rotations, sample #2 did not show a strain evolution exhibiting cyclic strain of about 60 ppm.

The interesting feature of the results presented in Fig. 8 is a training effect, i.e., a strong dependence of MFIS on the number of magneto-mechanical cycles. Despite the low absolute value of magnetostrain, this behavior suggests a magnetic field-induced structural changes, among them the most probable in the case under this study is the phenomenon of magnetic field-induced twin-boundary motion. The training effect provides a preliminary evidence of the existence of magnetic shape memory effect in non-modulated $L1_0$-ordered 2M-martensitic phase which was considered to be formed in the alloy #3 (Ref 9). Although the martensitic structure was not determined directly in this alloy, its superelastic properties are in agreement with the lattice parameters of non-modulated martensitic phase (Ref 9).

6. Summary

In this study, we found that increasing Co-content in the alloy $Ni_{54}Fe_{20-x}Co_xGa_{26}$ results in a considerable and regular change of its properties such as MT temperature, transformation hysteresis, Curie temperature, and saturation magnetization.

Selected alloys grown as the single crystals demonstrate a 4% tensile superelastic strain in as-grown state which is of interest for the applications. The temperature behaviors of the elastic modulus and internal friction in DMA measurements are similar to Ni-Mn-Ga alloys. The cyclic magnetostrain shows a training effect which is an evidence of the effect of magnetic field-induced twin-boundary motion.

Acknowledgments

This work was supported by Grant-in-Aid for Scientific Research from the Ministry of Education, Science, Sports and Culture, Japan, the Core Research for Evolution Science and Technology (CREST), Japan Science and Technology Agency (JST), and Fondazione Cariplo (2004.1819-A109251). PM and MC acknowledge financial support through the Department of Energy (DOE), Office of Basic Energy Sciences (BES) under Grant DE-FG-02-07ER46396. The authors are grateful to A. Gambardella and G. Carcano for technical assistance.

References

1. V.A. Chernenko, Ed., Advances in Shape Memory Materials: Ferromagnetic Shape Memory Alloys, *Mat. Sci. Forum*, **583**, TTP, Switzerland, 2008, 302 p
2. E. Cesari, J. Pons, R. Santamarta, C. Segui, and V.A. Chernenko, Ferromagnetic Shape Memory Alloys: An Overview, *Archiv. Metall. Mater.*, 2004, **49**, p 779–789
3. E. Cesari, J. Pons, C. Segui, and V.A. Chernenko, New Ferromagnetic Shape Memory Alloy Systems, *Applied Crystallography*, H. Moraviec and D. Stróz, Eds., World Scientific, 2004, p 128–133, ISBN 981-283-761-7
4. T. Oikawa, T. Ota, Y. Ohmori, H. Tanaka, A. Morito, R. Fujita, K. Kainuma, K. Fukamichi, and K. Ishida, Magnetic and Martensitic Phase Transitions in Ferromagnetic Ni-Fe-Ga Shape Memory Alloys, *Appl. Phys. Lett.*, 2002, **81**, p 5201–5203
5. H. Morito, A. Fujita, K. Fukamichi, R. Kainuma, K. Ishida, and K. Oikawa, Magnetic-field-induced Strain of Fe-Ni-Ga in Single-variant State, *Appl. Phys. Lett.*, 2003, **83**, p 4993–4995
6. T. Omori, N. Kamiya, Y. Sutou, K. Oikawa, R. Kainuma, and K. Ishida, Phase Transformations in Ni-Ga-Fe Ferromagnetic Shape Memory Alloys, *Mater. Sci. Eng. A*, 2004, **378**, p 403–408

7. K. Oikawa, Y. Imano, V.A. Chernenko, F. Luo, T. Omori, Y. Sutou, R. Kainuma, T. Kanomata, and K. Ishida, Influence of Co Addition on Martensitic and Magnetic Transitions in Ni-Fe-Ga—Based Shape Memory Alloys, *Mater. Trans.*, 2005, **46**, p 734–737
8. H. Morito, K. Oikawa, A. Fujita, K. Fukamichi, R. Kainuma K. Ishida, and T. Takagi, Effects of Partial Substitution of Co on Magnetocrystalline Anisotropy and Magnetic-field-induced Strain in NiFeGa Alloys, *J. Magn. Magn. Mater.*, 2005, **290–291**, p 850–853
9. K Oikawa, R Saito, K Anzai, H Ishikawa, Y Sutou, T Omori, K Ishida, R Kainuma, A Yoshikawa, VA Chernenko, S Besseghini, and A Gambardella, Elastic and Superelastic Properties of NiFeCoGa Single Crystals Grown by Micro-pulling-down Method, *Mat. Trans.*, 2009, **50**, p 934–937
10. P. Müllner, V.A. Chernenko, and G. Kostorz, Large Cyclic Magnetic-field-induced Deformation in Orthorhombic (14 M) Ni-Mn-Ga Martensite, *J. Appl. Phys.*, 2004, **95**, p 1531–1536
11. M. Chmielus, V.A. Chernenko, W.B. Knowlton, G. Kostorz, and P. Mullner, Training, Constraints, and High-cycle Magneto-mechanical Properties of Ni-Mn-Ga Magnetic Shape-memory Alloys, *Eur. Phys. J. Spec. Top.*, 2008, **158**, p 79–85
12. J. Pons, V.A. Chernenko, R. Santamarta, and E. Cesari, Crystal Structure of Martensitic Phases in Ni-Mn-Ga Shape Memory Alloys, *Acta Mater.*, 2000, **48**, p 3027–3038
13. H. Morito, K. Oikawa, A. Fujita, K. Fukamichi, R. Kainuma, and K. Ishida, Enhancement of Magnetic-field-induced Strain in Ni-Fe-Ga-Co Heusler Alloy, *Scripta Mater.*, 2005, **53**, p 1237–1241
14. J.M. Barandiarán, J. Gutiérrez, P. Lázpita, V.A. Chernenko, C. Seguí, J. Pons, E. Cesari, K. Oikawa, and T. Kanomata, Martensitic Transformation in Ni-Fe-Ga Alloys, *Mater. Sci. Eng. A*, 2008, **478**, p 125–129
15. V. Sanchez-Alarcoz, J.I. Perez-Landazabal, V. Recarte, C. Gomez-Polo, and J.A. Rodriges-Velamazan, Correlation Between Composition and Phase Transformation Temperatures in Ni-Mn-Ga Ferromagnetic Shape Memory Alloys, *Acta Mater.*, 2008, **56**, p 5370–5378
16. R.F. Hamilton, H. Sehitoglu, C. Efstahiou, H.J. Maier, and Y. Chumlyakov, Pseudoelasticity in Co-Ni-Al Single and Polycrystals, *Acta Mater.*, 2006, **54**, p 587–599
17. Y. Tanaka, K. Oikawa, Y. Sutou, T. Omori, R. Kainuma, and K. Ishida, Martensitic Transition and Superelasticity of Co-Ni-Al Ferromagnetic Shape Memory Alloys with $\beta + \gamma$ Two-phase Structure, *Mat. Sci. Eng. A*, 2006, **438–440**, p 1054–1060
18. Y. Sutou, N. Kamiya, T. Omori, R. Kainuma, and K. Ishida, Stress-strain Characteristics in Ni-Ga-Fe Ferromagnetic Shape Memory Alloys, *Appl. Phys. Lett.*, 2004, **84**, p 1275–1277
19. J. Gutierrez, P. Lázpita, V. Siruguri, J.M. Barandiarán, P. Henry, V.A. Chernenko, and T. Kanomata, Neutron Study of the Martensitic Transformation in Ni-Fe-Ga Alloys, *Int. J. Appl. Electromagn. Mech.*, 2006, **23**, p 71–74